PAPER Special Section on Heterostructure Microelectronics with TWHM2005

Structure-Sensitive Design for Wider Tunable Operation of Terahertz Plasmon-Resonant Photomixer

Mitsuhiro HANABE[†*a)], **Takuya NISHIMURA**[†*], *Student Members*, **Masaki MIYAMOTO**[†], *Nonmember*, **Taiichi OTSUJI**[††], *and* **Eiichi SANO**[†††], *Members*

SUMMARY We performed numerical analyses on structure sensitive field emission properties of our proposing plasmon resonant photomixer (PRX) in the terahertz range. The photomixer incorporates doubly interdigitated grating strips for gate electrodes and a vertical resonator structure for realizing highly efficient terahertz emission even at room temperature. We investigated the dependence of total field emission properties of PRX's on their material and dimension parameters. Introduction of low-conductive gate electrodes and ac-coupled 2D periodic plasmon gratings with depleted connecting portions are effective for expanding its lower cutoff frequency. The cutoff frequency, which is around 1.0 THz in standard metal-gates configuration, is expanded to less than 500 GHz. The output intensity could also be amplified more than double. On the other hand, a shorter vertical cavity is effective for expanding its upper cutoff frequency, which is expanded close to vertical resonant frequency, while maintaining the lower cutoff frequency. The combination of these design rules can realize much broader bandwidth operation.

key words: *plasmon resonance, photomixer, terahertz, grating, HEMT*

1. Introductuion

Recently, terahertz (THz) coherent electromagnetic waves are expected to open the new way for many technological applications such as imaging, spectroscopy, as well as future ubiquitous communication networks [1]–[6]. In 1993, Dyakonov and Shur demonstrated that two-dimensional (2D) electrons in the traveling channel of a submicron high-electron mobility transistor (HEMT) can make plasma resonant oscillation in the terahertz range [7]. Since that the plasma resonant effect has an important advantage; the resonant frequency is tunable by means of external gate bias voltage. This offers the possibility of a new frequency-tunable coherent terahertz wave source. So far, various analytical [6]–[15] and experimental studies [16]–[32] on the terahertz plasma-wave resonance have been emerging. Some studies demonstrated that the resonance can be excited by means of difference frequency generation (DFG) [12]–[15], [28], [30].

Manuscript received November 8, 2005.
Manuscript revised February 1, 2006.

[†]The authors are with the Graduate School of Computer Science and Systems Engineering, Kyushu Institute of Technology, Iizuka-shi, 820-8502 Japan.
[††]The author is with Research Institute of Electrical Communication, Tohoku University, Sendai-shi, 980-8577 Japan.
[†††]The author is with Research Center for Quantum Electronics, Hokkaido University, Sapporo-shi, 060-8628 Japan.
[*]Presently, with Research Institute of Electrical Communication, Tohoku University.
a) E-mail: hanabe@riec.tohoku.ac.jp
DOI: 10.1093/ietele/e89–c.7.985

Recently, we have proposed a device structure of highly efficient plasmon-resonant photomixer (PRX) [33]. The PRX is a compact solid-state source that photomixes two continuous wave (CW) laser inputs to generate a terahertz differential frequency. It is based on a normal HEMT device and incorporates two unique structures enabling highly efficient terahertz emission even at room temperature. The field emission properties of the PRX deeply depends on these device structures. In this paper, we numerically analyse its structure-sensitive field emission properties by using finite difference time domain (FDTD) method, and discuss a systematic procedure for optimizing of design parameters.

2. Plasmon Resonant Photomixer

2.1 Plasmon Resonance

When highly dense conduction electrons are transversely well confined in a field effect transistor (FET) channel, they behave as 2D electron fluid [7], [8]. Once two-photon were irradiated into the channel, the 2D electron fluid can make resonant oscillation under the standing wave conditions of the fundamental and odd harmonic modes for a common-source and open-drain configuration (see Fig. 1). The resonant condition is given by $\lambda = 4L_{ch}/(2l-1)$ (l: integer) where λ the plasma-wave length, L_{ch} the channel length. The resonant frequency f_r is determined by

$$f_r = \frac{(2l-1)v_p}{4L_{ch}}, \tag{1}$$

where v_p the plasma wave velocity given by

$$v_p = \sqrt{\frac{e^2 nd}{m_e \epsilon}}, \tag{2}$$

e the electronic charge, n the density of electrons, d the distance between the gate electrode and the gated 2D channel, m_e the electron effective mass, ϵ the permittivity. Since v_p is a function of n induced by the gate bias voltage V_{gs} (defined as an offset from the threshold voltage of the FET), f_r can be controlled by V_{gs}. In addition, in today's state-of-the-art sub-0.1-μm gate FET, the resonant frequency falls in the terahertz range. It is noted that the quality of resonant oscillation is evaluated by using a quality factor of $v_p\tau/L_{ch}$ where τ the plasma relaxation time. This factor should be

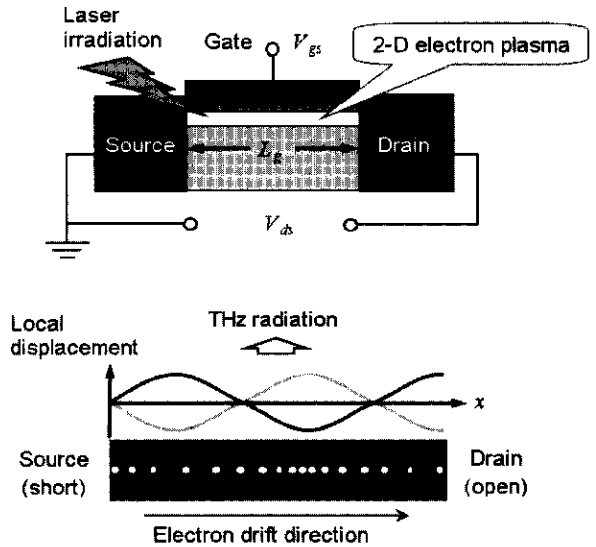

Fig. 1 Basic principle of the plasma-wave resonance in submicron channel of FET's. Under laser irradiation, highly dense conduction electrons can make resonant oscillation in the terahertz range.

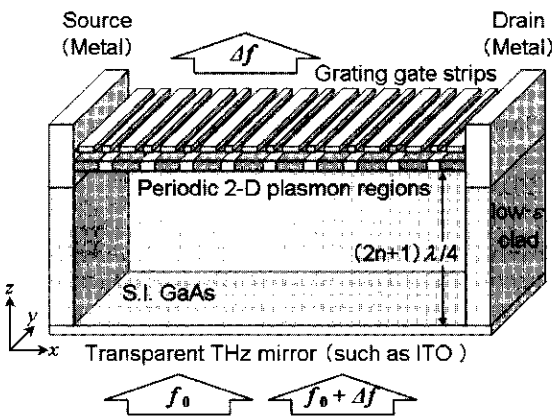

Fig. 2 Device cross section of the proposed 2D plasmon-resonant photomixer. Periodic plasmon regions and vertical resonator are introduced.

more than 1 for practical operation [8]. In such case, this resonant oscillation offers the possibility of FET-based tunable coherent terahertz oscillators.

2.2 Device Structure and Operation

Figure 2 shows the cross section of our proposing terahertz plasmon resonant photomixer [33]. The device structure is based on a HEMT and incorporates two unique features. One is doubly interdigitated grating strips for the gate electrodes that periodically localize the 2D electron systems (2DES) in sub 0.1-μm regions with a micron-order interval. This works as a terahertz antenna using a phenomenon like the well-known Smith-Purcell effect [34]. Another is a vertical cavity structure in between the top grating plane and a terahertz mirror at the back side. This works as an amplifier. The bottom terahertz mirror is a transparent metal like indium titanium oxide (ITO) making the plasmon excitation

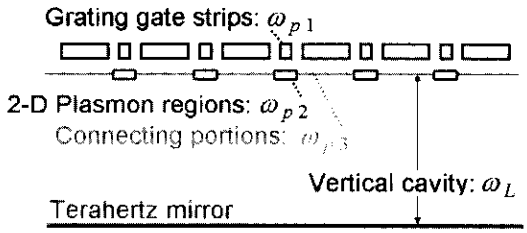

Fig. 3 Characteristic frequencies in the photomixer. ω_{p1}, ω_{p2} and ω_{p3} are determined by their grating materials and dimensions, and ω_L is determined by a length of the vertical cavity.

by optical two-photon irradiation from outside the back surface. The cladding guide with a low ϵ is an option for better confinement of the vertical cavity.

When co-linearly polarized two CW laser beams having slightly different frequencies (f_0 and $f_0 + \Delta f$) are absorbed in the 2D electron channel, photoexcited carriers and/or phonon-polariton modes can coherently excite the periodically locarized 2D plasmons, then they make resonant oscillation at the frequency of Δf. The plasmon waves themselves are non-radiative mode. The periodically localized 2D plasmons, however, can be coupled with those in neighbor regions and make in-phase resonant oscillation so that the 2D-plasmon grating can convert the non-radiative plasmon waves to radiative electromagnetic waves. This is attributed to the phenomena that the motion of a fast electron beam across a periodic metal structure results in the radiation of electromagnetic waves [34].

Once the terahertz electromagnetic waves are produced from the seed of plasmon waves, downward-propagating electromagnetic waves are reflected at the mirror back to the plasmon region so that the reflected waves can directly excite the plasmon again via inter-subband transition process. When the plasmon resonant frequency satisfies the standing wave condition of the vertical cavity, the terahertz electromagnetic radiation will reinforce the plasmon resonance in a recursive manner according to the Drude-optical conductivity [35]. Therefore, the vertical cavity may work as an amplifier if the gain exceeds the cavity loss.

2.3 Characteristic Frequencies

The field emission properties of the PRX are characterized by the structure dependent key parameters shown in Fig. 3. Each grating structure has its own characteristic frequency which affects the highest mode conversion gain and emission power [9]. These frequencies are determined by their material parameters and dimension parameters. At least our proposing PRX has three characteristic frequencies: (i) ω_{p1} of the gate electrodes, (ii) ω_{p2} of the 2D plasmon regions, and (iii) ω_{p3} of their connecting portions. According to Mikhailov [9], each characteristic frequency is given as

$$\omega_p^2 = \omega_p'^2\left[1 - \frac{(\pi f)^2}{24} - \frac{(\pi f)^4}{960}\right], \tag{3}$$

where ω_p' the plasma frequency, f the filling parameter

which is defined by the ratio of the single width of the material W to the periodic cycle a. For so-called *ungated* periodic structures, corrsponding to ω_{p1}, ω'_p is given as [9]

$$\omega'_p = \sqrt{\frac{16e^2n}{m_e\epsilon W}}. \tag{4}$$

On the other hand, for so-called *gated* periodic structures, corresponding to ω_{p2} and ω_{p3}, ω'_p is given as [7]

$$\omega'_p = \sqrt{\frac{e^2nd}{m_e\epsilon W^2}}. \tag{5}$$

According to the operating frequency band, the grating geometry (single plasmon cavity length and periodicity) is designed to be fixed ω_{p1} and ω_{p3} as well as ω_L are optimally designed. For an actual device operation, ω_{p2} is a given parameter, which is first tuned by the gate bias at the excitation frequency. As a fundamental design criterion to obtaining high quantum efficiency, ω_{p1} and ω_L values are to be matched to ω_{p2} value while ω_{p3} is far depart from them for a good plasmon resonance confinement. Once the device dimensions and material systems are designed, ω_{p1} and ω_L become fixed parameters. ω_{p3} for the connecting portion, on the other hand, is controllable so that one can set it at far higher or lower than ω_{p2} by making the connecting portion to be metallic or dielectric.

3. Numerical Analysis

3.1 Device Model

Figure 4 shows a virtual structure and typical parameters for our simulation. InGaP/InGaAs heterostructure material systems on a SI-GaAs substrate were assumed. The electron channel acting as a plasmonic cavity grating is formed with a 0.05-μm thick InGaAs buffer layer. Because of the limited memory space, nine periods of grating structures were modeled. The density of 2DES was periodically set as a pair of connecting and plasmonic cavity region corresponding to the gate gratings G1 and G2, respectively. The nominal conditions of the density of electrons n_2 and n_3 for the plasmonic cavity and connecting region are $1.0 \times 10^{12}\,\mathrm{cm}^{-2}$ and $1.0 \times 10^{14}\,\mathrm{cm}^{-2}$, respectively. The width of the plasmonic cavity W_2 and the connecting region W_3 were set at $0.1\,\mu$m and $1.9\,\mu$m, respectively, which gives the fundamental plasma frequency ω_{p2} of 3.4 THz for the plasmonic cavity region. The parameters for plasmonic regions give the condition of $v_p\tau/W_2 > 1$ at typical τ value of 0.1 ps for the InGaP/InGaAs HEMT channel in 300 K. This design offers room temperature operation. The doubly interdigitated gate strips, G1 and G2, are assumed to be quauntum wires [33] placed on top of the channel in a distance d of $0.1\,\mu$m. The width of G1 and G2, W_1 and W'_1, were set at $0.05\,\mu$m and $1.85\,\mu$m, respectively. It is noted that ω_{p1} has two values corresponding to G1 and G2. In this case, we set the nominal conditions of the density of electrons n_1 for the electrodes at $7.2 \times 10^{11}\,\mathrm{cm}^{-2}$ so as to coincide ω_{p1}(for G1) with ω_{p2}. Then ω_{p1}(for G2) cannot fall in the terahertz range of our interest due to the longer width of G2 itself, so we regard only ω_{p1}(for G1) as ω_{p1} to simplify the analysis in this paper. The thickness of the 2DES and the quantum wired gate gratings were set to be the minimum calculation lattice size of $0.01\,\mu$m. The vertical cavity length L_c was set at the quarter wavelength of ω_{p2}. The bottom surface was set either as the perfect electric boundary condition. The outer space is filled with air and all the outside boundary was set as the Mur's second-order absorbing boundary condition.

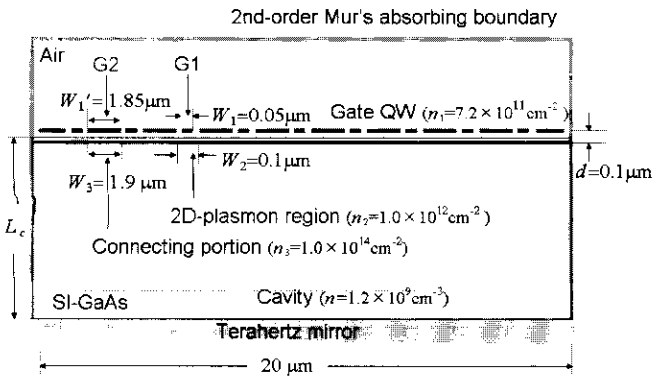

Fig. 4 Artificial device model for numarical simulation. The analytic space is closed by the perfect electrical conductor surface (bottom) and the 2nd-order Mur's absorbing boundary (others). QW: quantum wire.

3.2 Simulation

The plasma wave behavior of the 2DES is described by the extended Dyakonov-Shur model [7], [10]. Under the gradual channel approximation, the local density n and velocity v_p of the plasma fluid are formulated by the following hydrodynamic equations as time- and space-dependent variables:

$$m_e\left[\frac{\partial v_p}{\partial t} + (v_p \cdot \nabla)v_p\right] = -e\nabla V_{gc} - m_e\frac{v_p}{\tau}, \tag{6}$$

$$\frac{\partial n}{\partial t} + \nabla(nv_p) = \frac{\partial V_{gc}}{\partial t} + \nabla(V_{gc}v_p) = 0, \tag{7}$$

where V_{gc} the gate-to-channel potential. The transfer function for the plasma-wave excitation process is obtained from (6) and (7).

On the other hand, the transfer function for the THz field emission process from the plasma wave is obtained by Maxwell's equations. The electromagnetic component, parallel to the channel direction, is absorbed into the 2D layer. This leads to intersubband transition of 2D electrons and coherent plasmon excitation. The recursive process through the plasmon excitation to the electromagnetic emission/absorption can reinforce the total terahertz emission. This emission intensity is saturated depending on balance between the mode-conversion (non-radiative mode to radiative mode) efficiency of plasmons and the propagation losses inside the vertical cavity. Such a stimulated emission

process leads to a mode-conversion gain [33].

The total emission property is actually determined by the close relation between the hydrodynamic equations and Maxwell's equations. If the interaction between these equations, however, is not so strong, total emission properties can be simply described as a product of the two transfer functions.

In our PRX, photons are absorbed only at the plasmon layer so that the plasmon resonance is excited at the limited area. The former transfer function of plasmon resonance can be simply characterized by the two distinct parameters: the resonant frequency ω_{p2} and the damping factor τ according to Dyakonov-Shur's formula [8]. The latter THz field emission process of PRX is numerically analyzed in Sect. 3.3 by using Maxwell's FDTD simulator. After that, we will discuss the total device response in Sect. 3.4.

3.3 Results

In order to obtain the field emission properties of PRX, the impulse response simulation was conducted by using Maxwell's FDTD simulator. Impulsive current source parallel to the channel direction (x direction) was artificially put into each 2D plasmon region simultaneously. Since plasmons oscillate in x direction, our device outputs transverse electromagnetic (TEM) waves in which the x component of electric field E_x is dominant. Temporal response of E_x at the central point 4.0-μm above the gate electrode surface was Fourier transformed to show field emission spectra. (Through all results of this section, obtained spectrum distributions did not change except for intensity even if the monitoring point had been further separated from surface of the device.) In this simulation, ω_{p1}, ω_{p3} and ω_L were varied independently to discriminate each effect on the total field emission property of PRX.

Figure 5 shows the dependence of the field emission spectrum on the density n_1 of the gate electrodes. n_1 was set at five different levels from $2.1 \times 10^{12}\,\mathrm{cm}^{-2}$ (as high as general metal electrodes) down to $2.5 \times 10^{10}\,\mathrm{cm}^{-2}$ (below the density n_2 of the 2D plasmon regions). The nominal condition of $\omega_{p1} = 3.4\,\mathrm{THz}$ corresponds to the line for $n_1 = 7.2 \times 10^{11}\,\mathrm{cm}^{-2}$. Spectral peaks at just below 3.4 and 6.8 THz correspond to the fundamental and second harmonic mode of the vertical cavity resonance, respectively. With decreasing n_1, the peak intensity for the fundamental resonance was amplified, and the peak frequency shifted downward. This amplification mainly comes from decrease in the conductivity of the gate grating plane (depending on n_1) which determines wave-attenuation rate. The variation of peak frequency must reflect n_1 dependence of ω_{p1}. For verification, as shown in Fig. 6, we plotted peak frequencies versus n_1 as a parameter with ω_L, and compared them to ω_{p1} which is calculated from (3) and (4). The simulated fundamental peak frequencies fairly trace ω_{p1} in relatively low n_1 region. On the other hand, in highly dense region above $1.0 \times 10^{12}\,\mathrm{cm}^{-2}$, the peak frequency deviates from ω_{p1} and saturates to ω_L.

As recognized in this result, the emission property is given as a result of interaction between the characteristic frequencies. The final emission spectrum is strongly affected by ω_{p1}, ω_{p3} and/or ω_L, while plasmon resonant frequency is mainly governed by ω_{p2}. Structure-sensitive emission spectrum should be broaden so as to cover whole tunable range of ω_{p2}. This can be realized by utilizing the spectrum dependences on ω_{p1}, ω_{p3} and ω_L.

Figure 7 shows the dependence of the field emission spectrum on electron density n_3 of the connecting portions between the 2D plasmon regions. As mentioned before, n_3 must be far apart from the electron density of the plasmon regions n_2 ($= 1.0 \times 10^{12}\,\mathrm{cm}^{-2}$ in the nominal condition), thus there are two options: metallic and dielectric. The emission intensity at lower frequency regions was markedly improved for dielectric conditions with low n_3 values. It is considered to be due to the extreme downshift of ω_{p3}. Dielectric connecting portions can be realized by setting the gate bias voltage for G2 (in Fig. 4) to a sufficiently low level.

Figure 8 shows the dependence of the field emission spectrum on vertical resonant frequency ω_L. By shortening the vertical cavity length L_c, ω_L was detuned from the nominal value (3.4 THz) to 4.5 and 5.4 THz. As shown in

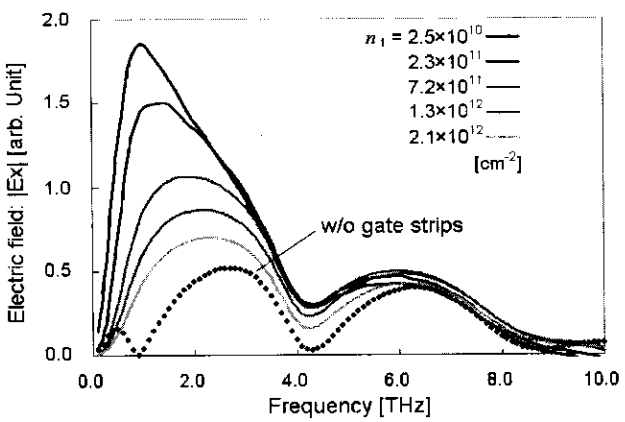

Fig. 5 The dependence of the field-emission spectrum on the electron density n_1 of the grating gate electrodes.

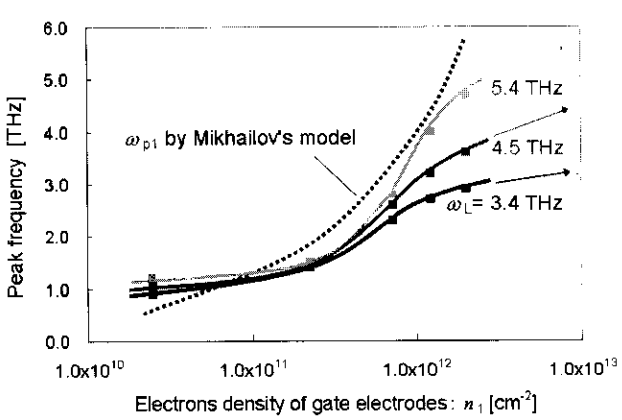

Fig. 6 Obtained peak frequencies vs. ω_{p1} which is calculated from Mikhailov's model (see (3) and (4)).

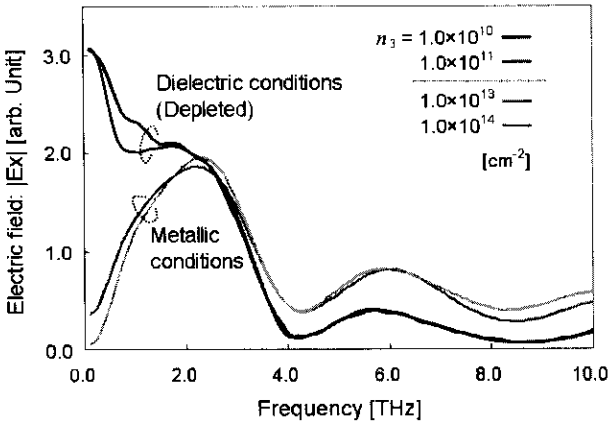

Fig. 7 The dependence of the field-emission spectrum on the electron density n_3 of the connecting portions.

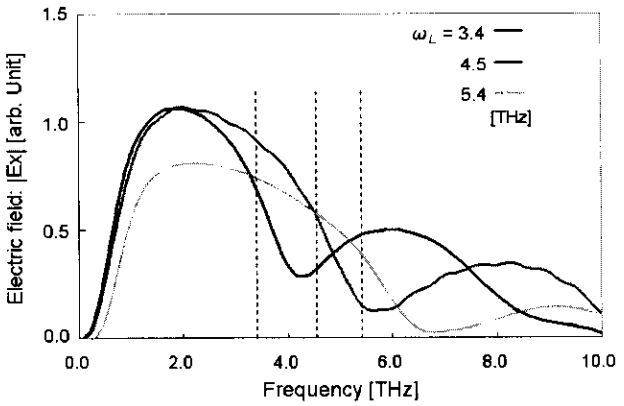

Fig. 8 The depencence of the field-emission spectrum on ω_L. The dotted lines show the selected ω_L values.

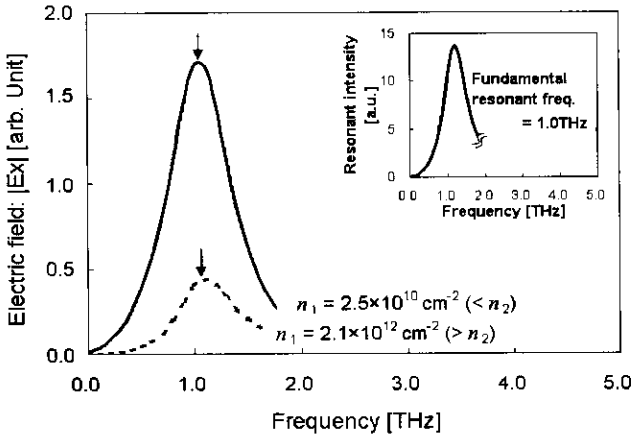

Fig. 9 The total field emission vs. n_1 for ω_{p2} (excitation frequency) = 1.0 THz.

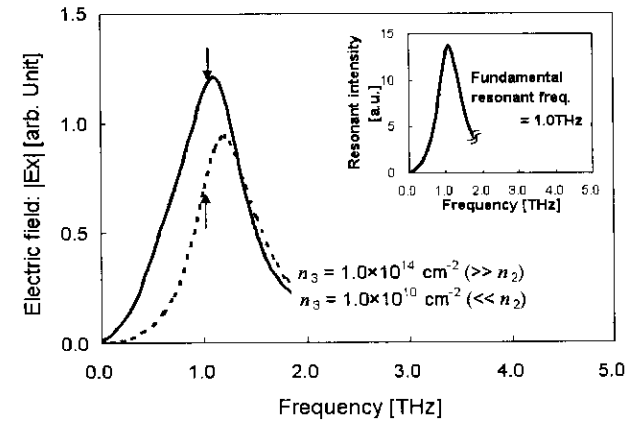

Fig. 10 The total field emission vs. n_3 for ω_{p2} (excitation frequency) = 1.0 THz.

Fig. 8, the higher cutoff frequency of the fundamental mode was shifted upward with increasing ω_L at the sacrifice of peak intensity, while maintaining the lower cutoff frequencies. Note that the higher cutoff frequencies are close to the given ω_L values.

3.4 Discussion

The total field emission response is approximately calculated as a product of the transfer function calculated in Sect. 3.3 and the transfer function of plasmon resonance excitation. We calculated the total emission properties of two focused regions: around 1.0 THz for the lower cutoff frequency and 3.6 THz for the higher cutoff frequency. In respective cases, n_2 was set at $3.5 \times 10^{10}\,\mathrm{cm}^{-2}$ and $3.1 \times 10^{11}\,\mathrm{cm}^{-2}$ so as to tune ω_{p2} to the plasmon excitation frequency.

At first, we set ω_{p2} at 1.0 THz. Figure 9 shows n_1 dependence of the total field emission spectra E_x. The inset shows the property of plasmon resonance excitation. In the lower n_1 condition, the emission intensity was markedly improved. Figure 10 shows n_3 dependence of E_x. Two curves corespond to the typical condition of connecting portions: metallic and dielectric, respectively. In the dielectric condition, the emission was amplified almost double. These results mean that low-conductive gate electrodes and depleted (dielectric) connecting portions are surely effective at lower frequency operation.

Next, we set ω_{p2} at 3.6 THz. Figure 11 shows ω_L dependence of E_x. The inset shows the property of plasmon resonant excitation. The total emission intensity was improved by tuning ω_L to the higher frequency. This results mean that detuning of ω_L from ω_{p2} are exactly effective at higher frequency operation.

Considering obtained results, we propose following structure-sensitive design procedures. (i) In terms of the enhancement of field emission intensity, low-n_1 conditions are preferable where the peak frequency is designable by the characteristic frequency ω_{p1}. The density of electrons deeply relates to the conductivity. A material for gate electrodes must be less conductive than 2D plasmon regions. Quantum wiring technology can realize the laying of anti-metal and low-conductive gate electrodes for that purpose. For example, a double heterostructure using an InGaP/InGaAs quantum well as gate electrodes is a con-

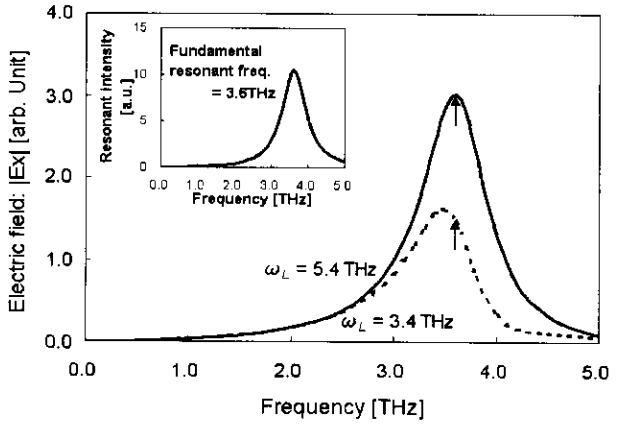

Fig. 11 The total field emission vs. ω_L for ω_{p2} (excitation frequency) = 3.6 THz.

siderable potential candidate. (ii) Connecting portions between 2D plasmon regions must be kept in depleted condition. This is realized also by setting the gate bias voltage for here to a sufficiently low level. (iii) A vertical cavity length should be detuned to the higher cutoff frequency of operation. The combination of these design rules can realize much broader bandwidth operation of our proposing PRX.

4. Conclusion

We performed numerical analyses on field emission properties of our proposing plasmon resonant photomixer in the terahertz range. Finite difference time domain simulation demonstrated that low-conductive gate electrodes and ac-coupled 2D periodic plasmon gratings with depleted connecting portions are effective for expanding its lower cutoff frequency. In addition, the higher cutoff frequency could be expanded by detuning the vertical resonant frequency to be higher than the characteristic frequency of plasmon regions. The combination of these design rules will realize much broader bandwidth operation.

Acknowledgement

The authors thank Prof. V. Ryzhii of University of Aizu, Prof. T. Asano of Kyushu Institute of Technology, and Dr. Y.M. Meziani of Tohoku University for their valuable discussion. This work was partially supported by the Strategic Information and Communications R&D Promotion Programme (SCOPE) from the Ministry of Internal Affairs and Communications, Japan.

References

[1] D.M. Mittleman, R.H. Jacobsen, and M.C. Nuss, "T-ray imaging," IEEE J. Sel. Top. Quantum Electron., vol.2, no.3, pp.679–691, Sept. 1996.

[2] S.P. Mickan and X.-C. Zhang, "T-ray sensing and imaging," Int. J. High Speed Electron. Syst., vol.13, no.2, pp.601–676, June 2003.

[3] C.M. Mann, "Towards terahertz communications systems," in Terahertz Sources and Systems, ed. R.E. Miles et al., pp.261–267, Kluwer Academic Publishers, Netherlands, 2001.

[4] S. Verghese, K.A. McIntosh, and E.R. Brown, "Highly tunable fiber-coupled photomixers with coherent terahertz output power," IEEE Trans. Microw. Theory Tech., vol.45, no.8, pp.1301–1309, Aug. 1997.

[5] H. Ito, F. Nakajima, T. Furuta, K. Yoshino, Y. Hirota, and T. Ishibashi, "Photonic terahertz-wave generation using antenna-integrated uni-travelling-carrier photodiode," Electron. Lett., vol.39, no.25, pp.1828–1829, Dec. 2003.

[6] T. Otsuji, S. Nakae, and H. Kitamura, "Numerical analysis for resonance properties of plasma-wave field-effect transistors and their terahertz applications to smart photonic network systems," IEICE Trans. Electron., vol.E84-C, no.10, pp.1470–1476, Oct. 2001.

[7] M. Dyakonov and M. Shur, "Shallow water analogy for a ballistic field effect transistor: New mechanism of plasma wave generation by DC current," Phys. Rev. Lett. vol.71, no.15, pp.2465–2468, Oct. 1993.

[8] M. Dyakonov and M. Shur, "Detection, mixing, and frequency multiplication of terahertz radiation by two-dimensional electron fluid," IEEE Trans. Electron Devices, vol.43, no.3, pp.380–387, March 1996.

[9] S.A. Mikhailov, "Plasma instability and amplification of electromagnetic waves in low-dimensional electron systems," Phys. Rev. B, vol.58, no.3, pp.1517–1532, July 1998.

[10] F.J. Crowne, "Contact boundary conditions and the Dyakonov-Shur instability in high electron mobility transistors," J. Appl. Phys., vol.82, no.3, pp.1242–1254, Aug. 1997.

[11] F.J. Crowne, "Dyakonov-Shur plasma excitations in the channel of a real high-electron mobility transistor," J. Appl. Phys., vol.87, no.11, pp.8056–8063, June 2000.

[12] V. Ryzhii, I. Khmyrova, and M. Shur, "Terahertz photomixing in quantum well structures using resonant excitation of plasma oscillations," J. Appl. Phys., vol.91, no.4, pp.1875–1881, Feb. 2002.

[13] V. Ryzhii and M. Shur, "Analysis of tunneling-injection transit-time effects and self-excitation of terahertz plasma oscillations in high-electron-mobility transistors," Jpn. J. Appl. Phys., vol.41, no.8B, pp.L922–924, Aug. 2002.

[14] V. Ryzhii, I. Khmyrova, A. Satou, P.O. Vaccaro, T. Aida, and M. Shur, "Plasma mechanism of terahertz photomixing in high-electron mobility transistor under interband photoexcitation," J. Appl. Phys., vol.92, no.10, pp.5756–5760, Nov. 2002.

[15] A. Satou, V. Ryzhii, I. Khmyrova, M. Ryzhii, and M.S. Shur, "Characteristics of a terahertz photomixer based on a high-electron mobility transistor structure with optical input through the ungated regions," J. Appl. Phys., vol.95, no.4, pp.2084–2089, Feb. 2004.

[16] S.J. Allen, Jr., D.C. Tsui, and R.A. Logan, "Observation of the two-dimensional plasmon in silicon inversion layers," Phys. Rev. Lett., vol.38, no.17, pp.980–983, April 1977.

[17] D.C. Tsui, E. Gornik, and R.A. Logan, "Far infrared emission from plasma oscillations of Si inversion layers," Solid State Commun., vol.35, no.11, pp.875–877, Sept. 1980.

[18] R.J. Wilkinson, C.D. Ager, T. Duffield, H.P. Hughes, D.G. Hasko, H. Armed, J.E.F. Frost, D.C. Peacock, D.A. Ritchie, A.C. Jones, C.R. Whitehouse, and N. Apsley, "Plasmon excitation and self-coupling in a bi-periodically modulated two-dimensional electron gas," J. Appl. Phys., vol.71, no.12, pp.6049–6061, June 1992.

[19] K. Hirakawa, K. Yamanaka, M. Grayson, and D.C. Tsui, "Far-infrared emission spectroscopy of hot two-dimensional plasmons in $Al_{0.3}Ga_{0.7}As$/GaAs heterojunctions," Appl. Phys. Lett., vol.67, no.16, pp.2326–2328, Oct. 1995.

[20] J.-Q. Lü, M. Shur, J.L. Hesler, L. Sun, and R. Weikle, "Terahertz detector utilizing two-dimensional electronic fluid," IEEE Electron Device Lett., vol.19, no.10, pp.373–375, Oct. 1998.

[21] N. Sekine, K. Yamanaka, K. Hirakawa, M. Voseburger, P. Haring-Bolivar, and H. Kurz, "Observation of terahertz radiation from higher-order two-dimensional plasmon modes in GaAs/AlGaAs single quantum wells," Appl. Phys. Lett., vol.74, no.7, pp.1006–1008, Feb. 1999.

[22] M. Shur and J.-Q. Lü, "Terahertz sources and detectors using two-dimensional electronic fluid in high-electron mobility transistors," IEEE Trans. Microw. Theory Tech., vol.48, no.4, pp.750–756, April 2000.
[23] X.G. Peralta, S.J. Allen, M.C. Wanke, N.E. Harff, J.A. Simmons, M.P. Lilly, J.L. Reno, P.J. Burke, and J.P. Einstein, "Terahertz photoconductivity and plasmon modes in double-quantum well field-effect transistors," Appl. Phys. Lett., vol.81, no.9, pp.1627–1629, Aug. 2002.
[24] W. Knap, Y. Deng, S. Rumyantsev, and M.S. Shur, "Resonant detection of subterahertz and terahertz radiation by plasma waves in submicron field-effect transistors," Appl. Phys. Lett., vol.81, no.24, pp.4637–4639, Dec. 2002.
[25] T. Otsuji, Y. Kanamaru, H. Kitamura, M. Matsuoka, and O. Ogawara, "Effects of heterostructure 2D-electron confinement on the tunability of resonant frequencies of terahertz plasma-wave transistors," IEICE Trans. Electron., vol.E86-C, no.10, pp.1985–1993, Oct. 2003.
[26] W. Knap, J. Lusakowski, T. Parenty, S. Bollaert, A. Cappy, V.V. Popov, and M.S. Shur, "Terahertz emission by plasma waves in 60 nm gate high electron mobility transistors," Appl. Phys. Lett., vol.84, no.13, pp.2331–2333, March 2004.
[27] D. Seliuta, E. Sirmulis, V. Tamosiunas, S. Balakauskas, S. Asmontas, A. Suziedelis, J. Gradauskas, G. Valusis, A. Lisauskas, H.G. Roskos, and K. Kohler, "Detection of terahertz/sub-terahertz radiation by asymmetrically-shaped 2DEG layers," Electron. Lett., vol.40, no.10, pp.631–632, May 2004.
[28] T. Otsuji, M. Hanabe, and O. Ogawara, "Terahertz plasma wave resonance of two-dimensional electrons in InGaP/InGaAs/GaAs high-electron-mobility transistors," Appl. Phys. Lett., vol.85, no.11, pp.2119–2121, Sept. 2004.
[29] M. Lee, M.C. Wanke, and J.L. Reno, "Millimeter wave mixing using plasmon and bolometric response in a double-quantum well field-effect-transistor," Appl. Phys. Lett., vol.86, no.033501, Jan. 2005.
[30] M. Hanabe, T. Otsuji, T. Ishibashi, T. Uno, and V. Ryzhii, "Modulation effects of photocarriers on the terahertz plasma-wave resonance in high-electron-mobility transistors under interband photoexcitation," Jpn. J. Appl. Phys., vol.44, no.6A, pp.3842–3847, June 2005.
[31] F. Teppe, D. Veksler, V.Y. Kachorovski, A.P. Dmitriev, X. Xie, S.-C. Xhang, S. Rumyantsev, W. Knap, and M. Shur, "Plasma wave resonant detection of femtosecond pulsed terahertz radiation by a nanometer field-effect transistor," Appl. Phys. Lett., vol.87, no.022102, July 2005.
[32] Y.M. Meziani, J. Lusakowski, N. Dyakonova, W. Knap, D. Seliuta, E. Sirmulis, J. Devenson, G. Valusis, F. Boeuf, and T. Skotnicki, "Non resonant response of terahertz radiation by submicron CMOS transistors," Dig. the 6th Topical Workshop on Heterostructure Microelectronics, no.TuC-6, pp.54–55, Awaji, Japan, Aug. 2005.
[33] T. Otsuji, M. Hanabe. J. Shigenobu, S. Takahashi, and E. Sano, "A novel plasma-wave photomixer with resonant-cavity enhanced structure," Tech. Dig. Int. Conf. on Terahertz Electronics, no.P1.16, pp.331–332, Karlsruhe, Germany, Sept. 2004.
[34] S.J. Smith and E.M. Purcell, "Visible light from localized surface charges moving across a grating," Phys. Rev., vol.92, no.4, p.1069, Nov. 1953.
[35] P.G. Huggard, J.A. Cluff, G.P. Moore, C.J. Shaw, S.R. Andrews, S.R. Keiding, E.H. Linfield, and D.A. Ritchie, "Drude conductivity of highly doped GaAs at terahertz frequencies," J. Appl. Phys., vol.87, no.5, pp.2382–2385, March 2000.

Mitsuhiro Hanabe was born in Fukuoka, Japan, in 1981. He received the M.E. degree in information science from Kyushu Institute of Technology, Fukuoka, 2004. He is presently with the Graduate School of Engineering, Tohoku University, and working toward the Ph.D. degree. He is a member of the Japan Society of Applied Physics.

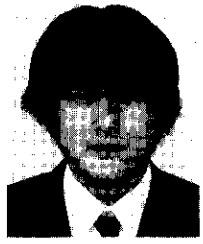

Takuya Nishimura was born in Saga, Japan, in 1981. He graduated from the Department of Control Engineering and Science, Faculty of Computer Science and Systems Engineering, Kyushu Institute of Technology in 2005. He is presently with the Graduate School of Engineering, Tohoku University, and working toward the M.E. degree.

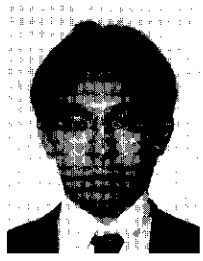

Masaki Miyamoto was born in Fukuoka, Japan, in 1981. He graduated from the Department of Control Engineering and Science, Faculty of Computer Science and Systems Engineering, Kyushu Institute of Technology in 2005. He is presently with the Graduate School of Information Science and Engineering, Kyushu Institute of Technology, and working toward the M.E. degree.

Taiichi Otsuji was born in Fukuoka, Japan, in 1959. He received the B.S. and M.S. degrees in electronic engineering from Kyushu Institute of Technology, Fukuoka, Japan, in 1982 and 1984, respectively, and the Ph.D. degree in electronic engineering from Tokyo Institute of Technology, Tokyo, Japan, in 1994. From 1984 through 1999, he worked for NTT Laboratories, Kanagawa, Japan, where he developed high-speed LSI test systems, ultra-high-speed optical communication ICs and ultrafast optoelectronic measurement systems. In 1999, he joined the Department of Control Engineering and Science, Faculty of Computer Science and Systems Engineering, Kyushu Institute of Technology, Fukuoka, Japan, as an associate professor. In 2005, he joined the Research Institute of Electric Communication, Tohoku University, Sendai, Japan, where he is currently a professor. He has been authored and co-authored more than 100 peer-reviewed journal papers and conference proceedings, and holds eight Japanese and three US patents. He is a member of the IEEE, OSA, and the Japan Society of Applied Physics.

Eiichi Sano was born in Shizuoka, Japan, in 1952. He received the B.S., M.S., and Ph.D. degrees from the University of Tokyo, Tokyo, Japan, in 1975, 1977, and 1998, respectively. From 1977 to 2001, he was with NTT Laboratories, where he worked on MOS device physics, mixed analog/digital MOS ULSIs, ultrafast MSM photodetectors, electro-optic sampling, and high-speed electronic and optoelectronic ICs. In 2001, he joined the Research Center for Integrated Quantum Electronics, Hokkaido University, Japan, as a professor. He has published more than 100 papers in major journals and conference proceedings related to these research areas. He is a member of IEEE, and the Japan Society of Applied Physics.